Catalysis Letters 81, No. 1-2 (2002) 25-31

Sulfated zirconia with ordered mesopores as an active catalyst for *n*-butane isomerization

X. Yang, F. C. Jentoft*, R. E. Jentoft, F. Girgsdies, T. Ressler

Department of Inorganic Chemistry, Fritz Haber Institute of the Max Planck Society,

Faradayweg 4-6, D-14195 Berlin, Germany

Abstract

Zirconia/surfactant composites were hydrothermally synthesized in aqueous sulfuric acid at 373 K using $Zr(O\text{-}nPr)_4$ as oxide precursor and hexadecyl-trimethyl-ammonium bromide (CTAB) as template. Mesostructural features similar to those of MCM-41 were detected by X-ray diffractometry, with d = 4.6 nm. A sample obtained from a starting mixture with Zr:S:CTAB = 2:2:1 was stable enough for removal of occluded organics. After calcination at 813 K, the d-value was 3.6 nm, the surface area 200 m^2/g, and the mean pore diameter estimated by the BJH method 2.2 nm. Extended X-ray absorption fine structure analysis suggests Zr to be in a short-range structure (< 4 Å) similar to that of Zr in monoclinic ZrO_2. Scanning electron microscopy including energy dispersive X-ray analysis showed 1-5 μm sulfur-containing ZrO_2 spheres. The material catalyzes the isomerization of *n*-butane to *i*-butane at 378 K with a steady activity in the order of magnitude of commercial sulfated ZrO_2.

Keywords: sulfated zirconia, mesoporous material, surfactant-templating synthesis, catalysis, *n*-butane isomerization, TG, SEM/EDX, EXAFS, XRD

* Corresponding author. Fax: +49-30-8413 4621

Introduction

The usage of supramolecular assemblies of amphiphiles as structure directing agents for the formation of M41S type materials [1] has been expanded in recent years to the syntheses of numerous non-siliceous oxides with ordered mesoporous structures [2], such as TiO_2 [3], WO_3 [4], Fe_2O_3 [5], $AlPO_4$ [6]. Zirconium dioxide, as a highly interesting support in heterogeneous catalysis [7], has also drawn much effort to be synthesized in mesoporous forms with ordered and narrowly distributed pores via amphiphile-templating. Many different surfactant templating routes using assemblies of cationic [8-16], anionic [17-22], and neutral [21,23] molecules with different hydrocarbon chain lengths have been applied for the preparation of mesostructured ZrO_2/organics composites from various zirconium compounds as the oxide precursors. Like the synthesis of other mesostructured oxide/surfactant composites, difficulties were encountered at the first stage to achieve the hexagonal packing of cylindrical pores similar to MCM-41 rather than the lamellar phase like MCM-50 [20-22]. And even if an MCM-41 structure has been realized for the as-synthesized materials, template-removal remains a challenge. It seems that the different coordination chemistry in comparison with silicon is one of the major reasons for the thermal instability; stable coordinated polyhedra of zirconium exist with the coordination number varying from 6 to 8. Furthermore, according to literature data, for zirconia/surfactant composites, the inorganic fraction is not as well condensed as in the case of siliceous MCM-41, and the organic/inorganic interaction is by contrast stronger. These facts together lead to pore collapse upon removal of the template, independently by means of calcination or through solvent extraction [9, 11-13, 17]. Following the pore collapse during calcination, ZrO_2 species transform into the monoclinic or tetragonal modification, just like the bulk crystallization of amorphous zirconium dioxide at temperatures above 773 K [24]. Fortunately, it has been found that sulfate [8,9,11-13] and

phosphate [9, 11-13, 17,18] species reinforce the bonding between zirconia fragments and delay the crystallization [20]. By tuning the sulfate contents in the starting mixtures or through a post-synthetic phosphate treatment it has been possible to obtain a zirconia/surfactant composite that possesses enough stability to undergo calcination to remove included template molecules and leave behind zirconia with ordered mesopores and amorphous pore walls [9-13].

On the other hand, zirconium dioxide, if modified with surface sulfate species, is known as an effective catalyst for *n*-butane isomerization. It is active at temperatures as low as room temperature and is usually employed below 523 K, where the branched alkane is thermodynamically preferred [25]. The catalyst is conventionally prepared by treating amorphous zirconium oxide hydrate with sulfate-containing solutions and subsequent calcination at elevated temperatures around 873 K. During the calcination complicated processes of dehydration, crystallization, and bonding of sulfate species onto the zirconia surface take place and result in materials consisting of tetragonal zirconia with small amounts of monoclinic contaminants. The specific surface area of the resulting catalyst is usually at around 80-100 m^2/g. Efforts have also been made to prepare sulfated zirconia catalysts consisting of the monoclinic phase [26], but an activity comparable to the catalysts with tetragonal ZrO_2 has never been achieved. This gives rise to the question of whether sulfated tetragonal zirconia is the sole active phase for this reaction [25]. Thus, it is interesting to test the activity of mesoporous zirconia with sulfate components for the isomerization of *n*-butane, because firstly, should this type of material be active, with its different morphology comparing to the conventional catalyst, it will be helpful to explain the mechanism of action of sulfated zirconia catalysts. Secondly, with its unique textural

properties such as a large surface area and porous structure, it may open up the possibility for a more economical use of the material.

Experimental Section

Sample preparation

In all experiments, hexadecyl-trimethyl-ammonium bromide (CTAB) was chosen as the template for the preparation of ZrO_2/surfactant composites. Synthetic procedures were adapted from the ones published by Ciesla et al. using zirconium *n*-propoxide as the oxide precursor [11]. As first step, 2.50 g (6.85 mmol) of CTAB (Fluka) were dissolved in a solution of 115.0 g water and 12.2 to 24.4 g 37 wt% HCl. Then 5.99 g (12.80 mmol) of 70 wt% $Zr(O\text{-}nPr)_4$ in 1-propanol (Aldrich) were slowly added under stirring. Hydrolysis products of $Zr(O\text{-}nPr)_4$ precipitated immediately upon contact with water. After ca. 0.5 h of stirring, the precipitates dissolved so that the slurry became a translucent sol. To this sol was added a solution of 0.85 to 1.69 g (6.43 to 12.80 mmol) $(NH_4)_2SO_4$ in 23.0 g water. The mixture was further stirred for 1 h, before it was sealed in a polypropylene bottle and heated to 373 K for 3 days under autogeneous pressure. Finally, the suspension was filtered, the solid products were washed with water, ethanol, and again with water, dried at 333 K overnight and calcined at 813 K for 16 h in air.

To compare the catalytic properties of the material obtained with that of traditional sulfated zirconia, two reference catalysts were prepared: 1) the commercially available catalyst MEL Cat. XZO682/01 from MEL Chemicals was calcined at 923 K in air for 3 h, and 2) $Zr(SO_4)_2 \bullet 4H_2O$ was calcined at 923 K as well. The latter method of preparation has been

demonstrated to yield a sulfated zirconia material that is active for *n*-butane isomerization [27]. Both reference catalysts consist of the tetragonal zirconia phase.

Characterization

X-ray diffractograms were recorded in theta-theta geometry on a STOE STADI-P X-ray diffractometer with a secondary monochromator and a scintillation counter, using Cu $K\alpha_{1,2}$ radiation (λ = 1.542 Å). The range of 2θ = 1 to 40° was scanned in steps of 0.02° (10 s per point) in order to gain information about the porous structure and the possible presence of bulk crystalline phases simultaneously. For the same reason, no antiscattering filter was used so that the diffractograms obtained have high baselines, especially in the small angle range.

X-ray absorption spectra were recorded at the Zr K edge (17.998 keV) at beamline X1.1 at the Hamburger Synchrotron Radiation Laboratory, HASYLAB, using a Si(311) double crystal monochromator. The storage ring operated at 3.6 GeV with injection currents of 150 mA. X-ray absorption fine structure (XAFS) analysis was performed using the software package WinXAS v2.1 [28]. Details about the XAFS analysis procedure employed can be found in reference [29]. EXAFS data analysis was carried out using theoretical backscattering phases and amplitudes calculated with the ab-initio multiple-scattering code FEFF7 [30]. Single scattering and multiple scattering paths in the employed model structures were calculated up to 4.1 Å with a lower limit of 2.0 % in amplitude with respect to the strongest backscattering path. EXAFS fitting and simulation were performed using the standard EXAFS formula (k range from 3.6 to 15.2 $Å^{-1}$, R range 1.1 to 4.2 Å). Refinements were carried out in R space to magnitude and imaginary part of a Fourier transformed k3-weighted experimental χ(k). Structural parameters refined are (i) E_0 shifts

for Zr and O backscatterers, (ii) Debye temperatures for Zr and O backscatterers, (iii) distances of single scattering shells with the same backscatterers in the monoclinic ZrO_2 structure that differ by less than 0.05 Å were constrained to vary the same in the refinement. Coordination numbers and S_0^2 were kept invariant in the refinement. The following crystallographic parameters were used for the calculations: monoclinic ZrO_2, SG: P 1 21/c 1 (14), a=5.169 Å, b=5.232 Å, c=5.342 Å, beta=99.3° [31]; tetragonal ZrO_2, SG: P 42/n m c Z (137), a=3.592 Å, c=5.184 Å [32]; cubic ZrO_2, SG: F M 3 M (225) a=5.09 Å [33].

Thermogravimetric and differential thermal analysis (TG-DTA) were carried out on a SEIKO microbalance with a heating rate of 10 K/min from room temperature to 1173 K. The sample was mounted horizontally and purged with a synthetic air flow of 100 ml/min.

Scanning electron microscopy and energy dispersive X-ray analysis (SEM-EDX) were performed on a Hitachi S-4000 Microscope equipped with a cold field emission gun and an energy dispersive X-ray detector. SEM images and EDX spectra were recorded with acceleration voltages from 3 kV to 15 kV.

Adsorption/desorption measurements were carried out using a Micromeritics TriStar 3000 automatic unit at 77 K with N_2 as adsorbate. Samples were outgassed at 423 K for 16 h in vacuum before the adsorption was started.

Catalytic tests

Catalytic tests were carried out in a flow-type fixed bed reactor with an internal diameter of 13 mm. 200.0 mg of catalyst powder were charged and activated at 723 K for 90 min in a

nitrogen flow of 30 ml/min. After cooling down to 378 K, a flow of 1 vol% *n*-butane in N_2 at a rate of 30 ml/min was fed at atmospheric pressure. Analysis was performed by on-line gas-chromatography using a Carboxen 1000 column (Supelco) and a flame ionization detector.

Results and Discussion

Preliminary experiments to synthesize ZrO_2/CTAB composites were carried out by varying H^+ and SO_4^{2-} concentrations in starting mixtures. It has been found that a ZrO_2/CTAB composite with MCM-41 structure can be readily synthesized from a starting mixture with Zr:S:CTAB = 2:4:1 (molar ratios) at pH = 1. However, consistent with literature data, the mesostructure of the composite collapses upon calcination at 813 K leading to the formation of sulfated tetragonal zirconia. Lowering the sulfate concentration in the starting mixture to Zr:S:CTAB = 2:1:1 while keeping the pH equal to 1, a similarly structured composite has been obtained which also transformed into sulfated tetragonal zirconia upon calcination. A thermally stable ZrO_2 framework can only be synthesized within a narrow range of synthetic variables. In our experiments a sample with a stable framework has been synthesized from a starting mixture containing 2.50 g CTAB, 5.99 g 70 wt% $Zr(O\text{-}nPr)_4$ in 1-propanol, 1.69 g $(NH_4)_2SO_4$, and 22.4 g 37 wt% HCl in 138.0 g H_2O (Zr:S:CTAB = 2:2:1). The pH of this mixture was ca. 1.

After calcination at 813 K in air, the sample has been subjected to a catalytic test of *n*-butane isomerization at 378 K. Under the applied conditions *i*-butane is the single reaction product over the mesoporous sample. The reaction rate of isomerization of *n*-butane is shown in Fig. 1 as a function of time on stream. The reaction test results of reference

catalysts with tetragonal modification, i.e., the MEL Chemicals catalyst and calcined $Zr(SO_4)_2$, are given in the same figure. It is observed that the activity of the mesoporous sample is higher than the calcined zirconium sulfate but much lower than that of the commercial sulfated zirconia. Both tetragonal catalysts pass through maxima of activity and deactivate quickly under the test conditions. By contrast, the mesoporous sample needs a longer induction time to reach the higher level of conversion, but it maintains the activity longer than both of the references do. The more stable activity is probably a contribution of the porous structure. Coke deposition could be restricted in the mesopores, and thus deactivation slows down. This is the first time that it has been demonstrated that a sulfur-containing mesoporous zirconia, with a morphology quite different from conventional sulfated zirconia catalysts, possesses an activity for *n*-butane isomerization, which is at a comparable order of magnitude to that of the conventional catalysts. To explain these catalytic performances of the synthesized sample, full characterization is required.

The X-ray diffractograms of both the as-synthesized and the calcined form of the sample are given in Fig. 2. The as-synthesized sample exhibits only one XRD peak at d = 4.6 nm, with no diffraction peaks corresponding to condensed crystalline ZrO_2 phases. After calcination, the peak has shifted to d = 3.6 nm but remains well resolved. In the 2θ range of 4 – 7°, where the higher indexed peaks should be present assuming hexagonal ordering, two weak diffraction peaks are observed. No peaks of the tetragonal or monoclinic zirconia phase appear at 2θ around 30°, indicating that no bulk crystallites of zirconia phases were formed during calcination. After the reaction test, the sample recovered from the reactor has been subjected to the XRD measurement again. The diffractogram remains largely unchanged. In the TG/DTA curves (Fig. 3) it is seen, that the burning-out of the template was completed below 750 K, it was associated with weight loss and an exotherm. A further

weight loss with endothermic effects is observed at 950 K, and is attributed to the decomposition of strongly bonded sulfate species. Below 850 K there is no significant exothermic heat flow signal that can be assigned to crystallization of a ZrO_2 phase. The TG data thus confirm the XRD results, i.e. the sample calcined at 813 K does not contain monoclinic or tetragonal zirconia crystallites of a detectable size.

Adsorptive properties of the calcined sample have been characterized by N_2 adsorption/desorption at 77 K. The results are shown in Fig. 4. It is an isotherm of type IV [34], with a steep increment of the adsorbed volume at low pressure and a second one at P/P_0 around 0.2, corresponding to pore filling. A hysteresis between the adsorption and desorption branches is insignificant. This is typical for a mesoporous material with narrowly distributed pore diameters, which are not far above 2 nm. Applying the BJH method [35] to the desorption data to estimate the pore diameter, a sharp maximum was found at ca. 2.2 nm. Comparing this value with the mean lattice distance obtained by XRD (d = 3.6 nm), the average thickness of pore walls can be calculated roughly as 1 nm. The BET specific surface area, calculated from the adsorption data in the range of P/P_0 =0.05 to 0.15, is 202 m^2/g, i.e, ca. 25250 m^2/mol. In comparison, Si-MCM-41, which is synthesized using the same template possesses usually a BET specific surface area of around 1000 m^2/g, or 60000 m^2/mol [36]. If normalized to the bulk density of ZrO_2 versus SiO_2 (ca. 5:2), these values are comparable in the same order of magnitude.

SEM images of the calcined sample are depicted in Fig. 5, as well as EDX spectra recorded at different locations on the sample particles. An overview reveals that the sample consists of particles with identical morphology, specifically spheres; aggregates of such spheres were also observed. Most of the spherical particles had a diameter of ca. 2 μm, but there

were also some others with diameters throughout the range of 1 to 5 μm. Plate-like aggregates were also found, though seldom, and it is believed that they are formed through intergrowth of the spheres. EDX analysis at various positions, e.g., at the sphere shell and in the core of broken spheres, as well as at the surface of a plate-like aggregate, showed that sulfur species are quite homogeneously integrated in the particles, with an average of 5 wt% S throughout the sample. The fact that the particles possess spherical morphology provides an explanation to the weak and broad XRD peaks in the 2θ range of 4-7°. Recently published diffractograms of a new modification of siliceous MCM-41 with spherical morphology [37] also show no distinct higher order reflexes. The authors argue that hexagonal packing of the pores is seen only within short ranges in a spherical particle while the long-range order is disturbed.

Efforts have also been made to perform transmission electron microscopy on the calcined sample. Unfortunately, a clear imaging of a porous pattern has not yet been achieved. The ZrO_2 forming the pore walls appeared amorphous, giving no electron diffraction pattern in the cores of the spherical particles and, at the beginning of the microscopic experiment, at the sphere shells, either. But within the shortest time under the electron beam, the sphere shells began to crystallize into the tetragonal and the monoclinic zirconia condensed phases. The sphere cores survive the electron-beam somewhat longer, but it has not been possible to take a TEM image due to the large thickness.

EXAFS investigations gave more insight into the nature of the walls. Fig. 6 shows FT(χ(k)) of the sample in as-synthesized and calcined form obtained by experiment, and FT(χ(k)) for cubic, tetragonal, and monoclinic zirconia (c-, t-, m-ZrO_2) obtained by calculation using model structures and FEFF. By applying Zr and O Debye temperatures

for the three model systems similar to those obtained in the XAFS refinement, the amplitude of the Fourier transforms was tailored to match that of the experimental data. A satisfactory XAFS fit to the experimental χ(k) of the as-synthesized sample required a mixture of 70 % m-ZrO_2 and 30 % t-ZrO_2. The calcined form could be sufficiently described by modification of an m-ZrO_2 structure as shown in Fig. 7, and indicating a local (< 4 Å) structure significantly less well ordered than that of cubic or tetragonal zirconia. The Zr-O coordination in the first shell of the as-synthesized and the calcined sample did not change significantly upon calcination, but a slight contraction of the Zr-Zr distances in the higher shells occurred (Table 1). For the calcined sample, the data exclude the presence of tetragonal crystallites of a size below the XRD detection limit. Given the thinness of the walls, a large fraction of zirconium atoms are surface atoms and are expected to have a coordination that is incomplete or different from the bulk, at least in the second shell (Zr-Zr). Consistent with this picture, the data are most similar to the least symmetric reference, i.e. the monoclinic modification of ZrO_2.

The characterization results allow the conclusion that the calcined sample possesses the expected mesoporous structure with narrowly distributed pore diameters. The morphology of the sample is quite different from the ones of conventional sulfated zirconia catalysts, without bulk crystalline zirconia phases as constituents. The sample contains sulfur species, hence it exhibits catalytic activity for *n*-butane isomerization to *i*-butane. The reaction profile of the mesoporous materials differs from that of commercial sulfated zirconia. The mesoporous material does neither display a maximal activity at short time on stream nor does it deactivate within the observation span. Rather, its activity increases slowly and reaches the same level as that of the commercial sulfated zirconia after ca. 1000 min on stream. A model explaining the behavior of both catalysts would include the

presence of some highly active sites only in conventional sulfated zirconia, which are responsible for the high short term activity. Because sulfated mesoporous zirconia, which basically consists only of walls, displays no such short term activity, it appears that the presence of the highly active sites is linked to the presence of a crystalline zirconia bulk. Conventional and mesoporous sulfated zirconia are similar in their long term activity, suggesting the presence of similar, moderately active sites on both materials. Experiments to confirm this hypothesis are currently underway in our laboratory.

Acknowledgements

B. Bems, E. Kitzelmann, Dr. V. V. Roddatis, G. Weinberg at the Fritz Haber Institute, and Dr. J.-G. Jia, Dr. R. A. Caruso at the Max Planck Institute of Colloids and Interfaces are thanked for their help in characterizing the samples, Prof. R. Schlögl for long-lasting supports.

References

[1] C. T. Kresge, M. E. Leonowicz, W. J. Roth, J. C. Vartuli, Nature 359 (1992) 710.

[2] A. Monnier, F. Schüth, Q. Huo, D. Kumar, D. Mongolese, R. S. Maxwell, G. D. Stucky, M. Krishnamurty, P. Petroff, A. Firouzi, M. Janicke, B. F. Chmelka, Science 261 (1993) 1299.

[3] D. M. Antonelli, J. Y. Ying, Angew. Chem. 107 (1995), 2202; Angew. Chem. Int. Ed. Eng. 34 (1995) 2014.

[4] Q. Huo, D. Magoless, T. E. Gier, P. Siege, R. Leon, P. Petroff, F. Schüth, G. D. Stucky, Nature 368 (1994), 317.

[5] G. Wirnsberger, K. Gatterer, H. P. Fritzer, W. Grogger, B. Pillep, P. Behrens, M. F. Hansen, C. Bender Koch, Chem. Mater. 13 (2000) 1453.

[6] T. Kimure, Y. Sugahara, K. Kuroda, Chem. Lett. (1997) 983.

[7] K. Tanabe, Mater. Chem. Phys. 13 (1985) 347.

[8] J. S. Reddy, A. Sayari, Catal. Lett. 38 (1996) 219.

[9] U. Ciesla, S. Schacht, G. D. Stucky, K. K. Unger, F. Schüth, Angew. Chem. 108 (1996) 597; Angew. Chem. Int. Ed. Eng. 35 (1996) 541.

[10] V. N. Romannikov, V. B. Fenelonov, E. A. Paukshtis, A. Yu. Derevyankin, V. I. Zaikovskii, Microporous and Mesoporous Materials 21 (1998) 411.

[11] U. Ciesla, M. Fröba, G. Stucky, F. Schüth, Chem. Mater. 11 (1999) 227.

[12] F. Schüth, U. Ciesla, S. Schacht, M. Tieme, Q. Huo, G. Stucky, Mater. Res. Bull. 34 (1999) 483.

[13] M. Lindén, J. Blanchard, S. Schacht, S. A. Schunk, F. Schüth, Chem. Mater. 11 (1999) 3002.

[14] M. Mamak, N. Coombs, G. Ozin, Adv. Mater. 12 (2000) 198.

[15] H.-R. Chen, J.-L. Shi, J. Yu, L.-Z. Wang, D.-S. Yan, Microporous and Mesoporous Materials 39 (2000) 171.

[16] V. I. Pârvulescu, V. Pârvulescu, U. Endruschat, C. W. Lehman, P. Grange, G. Poncelet, H. Bönnemann, Microporous and Mesoporous Materials 44-45 (2001) 221.

[17] M. S. Wong, D. M. Antonelli, J. Y. Ying, NanoStructured Materials 9 (1997) 165.

[18] M. S. Wong, J. Y. Ying, Chem. Mater. 10 (1998) 2067.

[19] D. M. Antonelli, Adv. Mater. 11 (1999) 487.

[20] Y. Huang, W. M. H. Sachtler, Chem. Commun. (1997) 1181.

[21] G. Pacheco, E. Zhao, E. Diaz Valdes, A. Garcia, J. J. Fripiat, Microporous and Mesoporous Materials 21 (1999) 175.

[22] G. Pacheco, J. J. Fripiat, J. Phys. Chem. 104 (2000) 11906.

[23] Y.-Y. Huang, T. J. McCarthy, W. M. H. Sachtler, Appl. Catal. A: General 148 (1996) 135.

[24] N. K. Simha, Journal de Physique IV 5 (1995) C8-1121.

[25] X. Song, A. Sayari, Catal. Rev. – Sci. Eng. 38 (1996) 329.

[26] J. B. Laizet, A. K. Søiland, J. Leglise, J. C. Duchet, Topics in Catalysis 10 (2000) 89.

[27] K. Arata, M. Hino, N. Yamagata, Bull. Chem. Soc. JPN. 63 (1990) 244.

[28] T. Ressler, J. Synch. Rad. 5 (1998) 118.

[29] T. Ressler, S. L. Brock, J. Wong, S. L. Suib, J. Phys. Chem. B 103 (1999) 6407.

[30] J. J. Rehr, C. H. Booth, F. Bridges, S. I. Zabinsky, Phys. Rev. B 49 (1994) 12347.

[31] J. D. McMullough, Acta Cryst. 1 (1967) 1948.

[32] C. J. Howard, E. H. Kisi, R. B. Roberts, R. J. Hill, J. Am. Ceram. Soc. 73 (1990) 2828.

[33] G. Katz, J. Am. Ceram. Soc. 54 (1971) 531.

[34] S. J. Gregg, K. S. W. Sing, *Adsorption, Surface Area and Porosity, 2. Ed.* (Academic Press, London, 1982).

[35] E. P. Barrett, L. G. Joyner, P. P. Halenda, J. Am. Chem. Soc. 73 (1951) 373.

[36] M. Selle, S. Ernst, Microporous and Mesoporous Materials 27 (1999) 355.

[37] B. Pauwels, G. Van Tendeloo, C. Thoelen, W. Van Rhijn, P. Jacobs, Advanced Materials, 13 (2001) 1317.

Table 1: Atomic distances Zr-O and Zr-Zr from EXAFS

Pair	CN	R [Å]		
		calcined	composite	m-ZrO_2
Zr–O	1	2.06	2.10	2.042
Zr–O	1	2.07	2.12	2.100
Zr–O	1	2.12	2.16	2.151
Zr–O	1	2.15	2.19	2.159
Zr–O	1	2.16	2.20	2.181
Zr–O	1	2.26	2.26	2.264
Zr–O	1	2.29	2.29	2.264
Zr–Zr	1	3.24	3.34	3.351
Zr–Zr	2	3.40	3.52	3.456
Zr–Zr	2	3.41	3.53	3.476
Zr–Zr	1	3.42	3.53	3.493
Zr–Zr	1	3.38	3.49	3.591
Zr–Zr	2	3.76	4.01	3.946
Zr–Zr	2	3.84	4.10	4.046

Parameters for calculations of EXAFS with FEFF:
as synthesized: $\Theta(Zr) = 780$ K, $\Theta(O) = 225$ K, $E_0(Zr) = -6.0$ eV, $E_0(O) = -3.1$ eV, $S_o^2 = 1.0$
calcined: $\Theta(Zr) = 800$ K, $\Theta(O) = 230$ K, $E_0(Zr) = -4.7$ eV, $E_0(O) = -2.9$ eV, $S_o^2 = 1.0$

Fitting parameters: number of independent parameters: 25; number of free running parameters: 14; number of single scattering paths: 21; number of multiple scattering paths: 31.

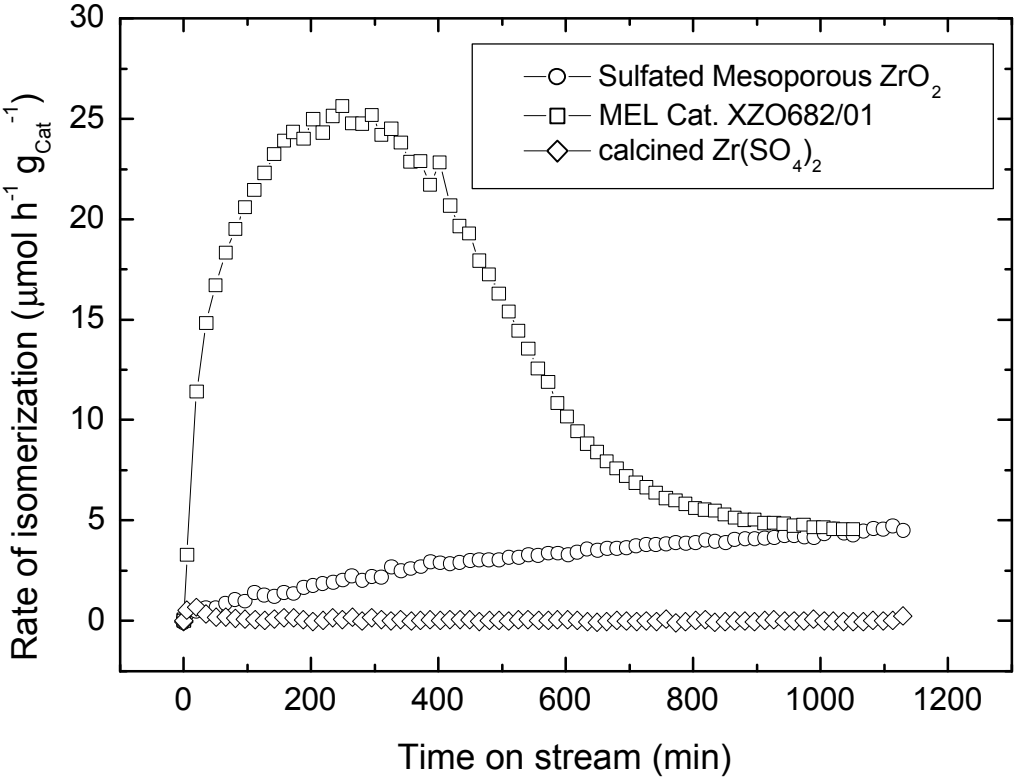

Figure 1: Reaction test results of a) the ZrO_2/CTAB composite synthesized using $Zr(O\text{-}nPr)_4$ with Zr:S:CTAB = 2:2:1 in the starting mixture, calcined at 813 K, b) MEL Cat. XZO682/01, and c) calcined $Zr(SO_4)_2$. Each test was carried out with 200 mg catalysts at 378 K, 1 vol% *n*-butane in N_2, total flow 30 ml/min, at atmospheric pressure.

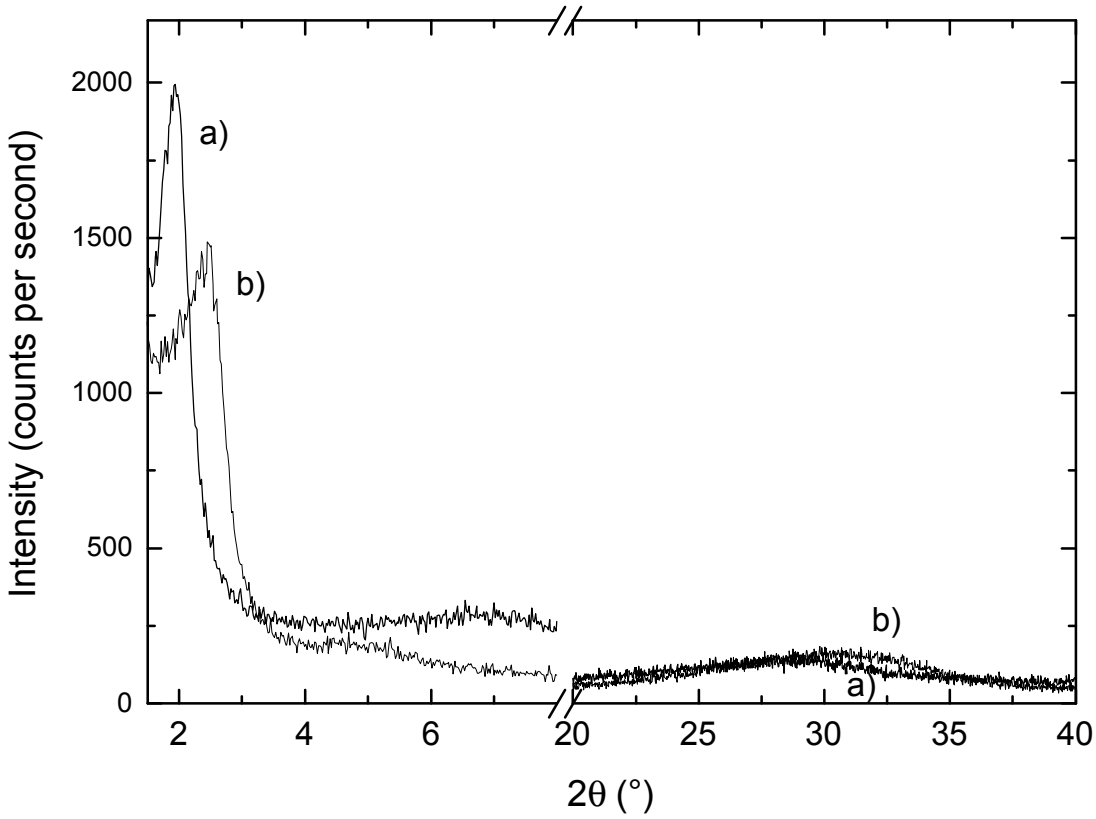

Figure 2: XRD patterns of a sample synthesized with $Zr(O\text{-}nPr)_4$ and CTAB with Zr:S:CTAB = 2:2:1 in the starting mixture: a) as-synthesized and b) calcined at 813 K in air.

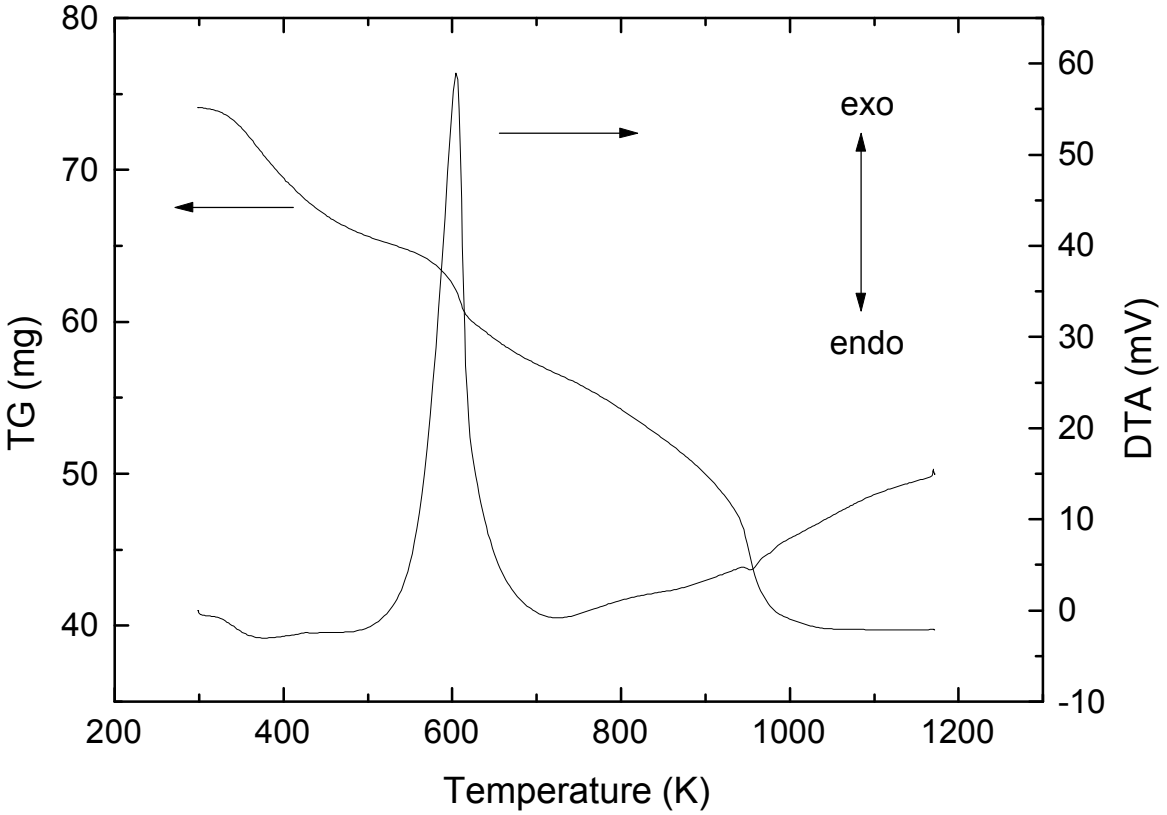

Figure 3: TG/DTA curves for the ZrO_2/CTAB composite synthesized with $Zr(O\text{-}nPr)_4$ in the presence of sulfate ions at Zr:S:CTAB = 2:2:1, measured with 10 K/min in an air stream.

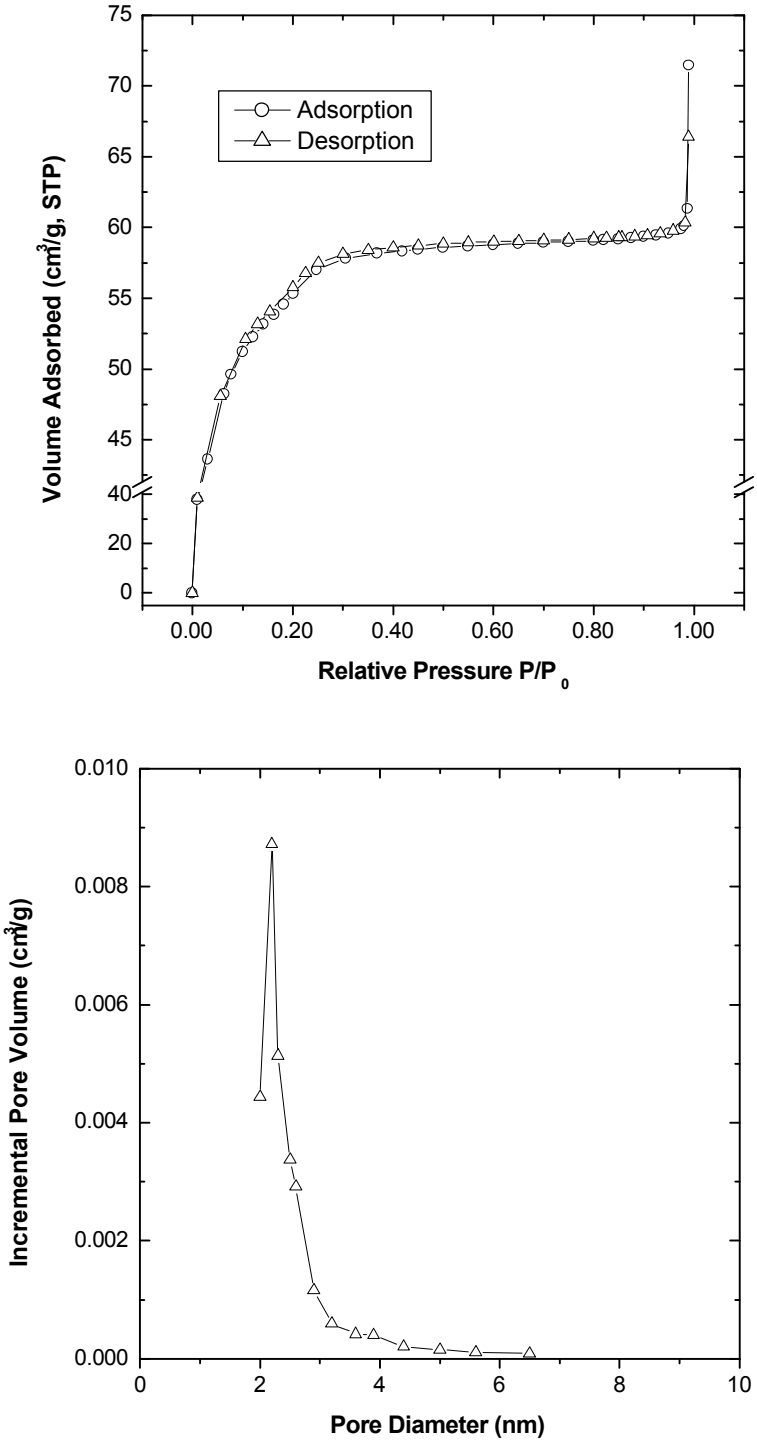

Figure 4: N_2 adsorption/desorption isotherm at 77 K of the ZrO_2/CTAB composite synthesized with $Zr(OPr)_4$ in the presence of sulfate ions and calcined at 813 K, BJH pore diameter distribution calculated from the desorption data.

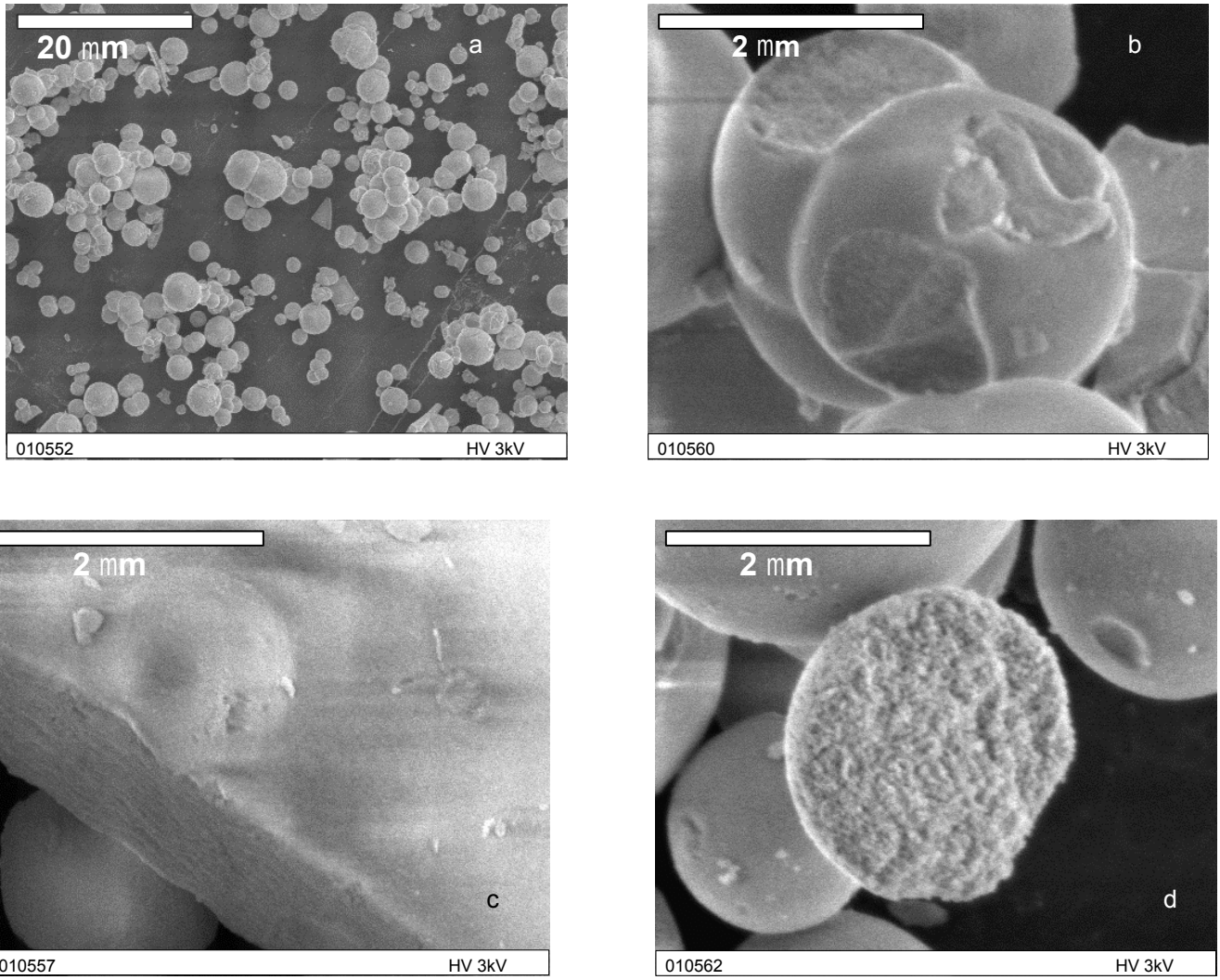

Figure 5: SEM images of the ZrO_2/CTAB composite synthesized using $Zr(OPr)_4$ with Zr:S:CTAB = 2:2:1 in the starting mixture and calcined at 813 K: a) an overview, b) an enlargement of the spherical particles, c) a plate-like aggregate, d) a broken sphere. The EDX spectra: e) at the sphere surface, f) at the surface of the plate-like aggregate and g) in the core of a broken sphere.

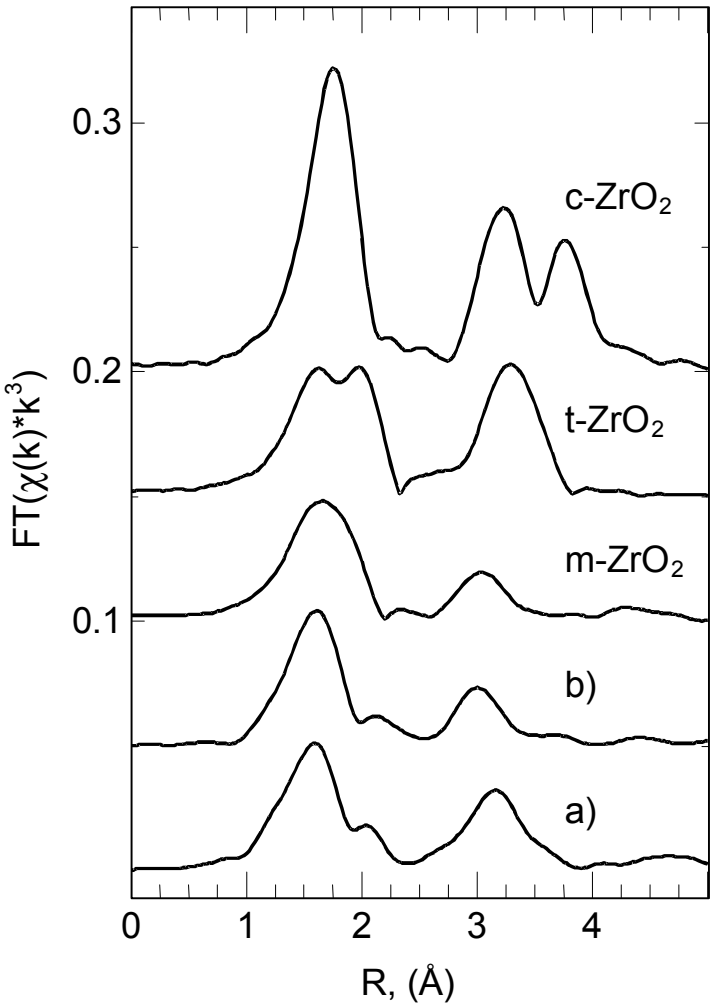

Figure 6: Zr K edge EXAFS of the a) as-synthesized and b) calcined sample synthesized using $Zr(O\text{-}nPr)_4$ with Zr:S:CTAB = 2:2:1 in the starting mixture, as obtained from experiments. For comparison, cubic, tetragonal, and monoclinic zirconia (c-, t-, m-ZrO_2), calculated using model structures.

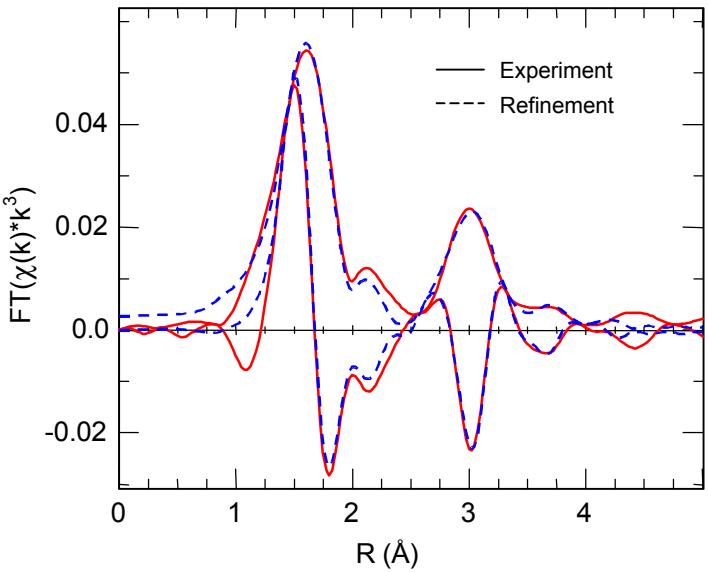

Figure 7: EXAFS refinement to the spectrum of the calcined sample. Sample synthesized using $Zr(O\text{-}nPr)_4$ with Zr:S:CTAB = 2:2:1 in the starting mixture.